



<http://www.diva-portal.org>

This is the published version of a paper published in *Physical Review Letters*.

Citation for the original published paper (version of record):

Ablikim, M., Achasov, M N., Ai, X C., Albayrak, O., Albrecht, M. et al. (2015)
Measurement of the Absolute Branching Fraction for $\Lambda^+(c) \rightarrow \Lambda e^+ \nu(e)$.
Physical Review Letters, 115(22): 221805
<http://dx.doi.org/10.1103/PhysRevLett.115.221805>

Access to the published version may require subscription.

N.B. When citing this work, cite the original published paper.

Permanent link to this version:

<http://urn.kb.se/resolve?urn=urn:nbn:se:uu:diva-271437>

Measurement of the Absolute Branching Fraction for $\Lambda_c^+ \rightarrow \Lambda e^+ \nu_e$

M. Ablikim,¹ M. N. Achasov,^{9,f} X. C. Ai,¹ O. Albayrak,⁵ M. Albrecht,⁴ D. J. Ambrose,⁴⁴ A. Amoroso,^{49a,49c} F. F. An,¹ Q. An,^{46,a} J. Z. Bai,¹ R. Baldini Ferroli,^{20a} Y. Ban,³¹ D. W. Bennett,¹⁹ J. V. Bennett,⁵ M. Bertani,^{20a} D. Bettoni,^{21a} J. M. Bian,⁴³ F. Bianchi,^{49a,49c} E. Boger,^{23,d} I. Boyko,²³ R. A. Briere,⁵ H. Cai,⁵¹ X. Cai,^{1,a} O. Cakir,^{40a,b} A. Calcaterra,^{20a} G. F. Cao,¹ S. A. Cetin,^{40b} J. F. Chang,^{1,a} G. Chelkov,^{23,d,e} G. Chen,¹ H. S. Chen,¹ H. Y. Chen,² J. C. Chen,¹ M. L. Chen,^{1,a} S. J. Chen,²⁹ X. Chen,^{1,a} X. R. Chen,²⁶ Y. B. Chen,^{1,a} H. P. Cheng,¹⁷ X. K. Chu,³¹ G. Cibinetto,^{21a} H. L. Dai,^{1,a} J. P. Dai,³⁴ A. Dbeysy,¹⁴ D. Dedovich,²³ Z. Y. Deng,¹ A. Denig,²² I. Denysenko,²³ M. Destefanis,^{49a,49c} F. De Mori,^{49a,49c} Y. Ding,²⁷ C. Dong,³⁰ J. Dong,^{1,a} L. Y. Dong,¹ M. Y. Dong,^{1,a} Z. L. Dou,²⁹ S. X. Du,⁵³ P. F. Duan,¹ J. Z. Fan,³⁹ J. Fang,^{1,a} S. S. Fang,¹ X. Fang,^{46,a} Y. Fang,¹ L. Fava,^{49b,49c} O. Fedorov,²³ F. Feldbauer,²² G. Felici,^{20a} C. Q. Feng,^{46,a} E. Fioravanti,^{21a} M. Fritsch,^{14,22} C. D. Fu,¹ Q. Gao,¹ X. L. Gao,^{46,a} X. Y. Gao,² Y. Gao,³⁹ Z. Gao,^{46,a} I. Garzia,^{21a} K. Goetzen,¹⁰ W. X. Gong,^{1,a} W. Gradl,²² M. Greco,^{49a,49c} M. H. Gu,^{1,a} Y. T. Gu,¹² Y. H. Guan,¹ A. Q. Guo,¹ L. B. Guo,²⁸ Y. Guo,¹ Y. P. Guo,²² Z. Haddadi,²⁵ A. Hafner,²² S. Han,⁵¹ X. Q. Hao,¹⁵ F. A. Harris,⁴² K. L. He,¹ T. Held,⁴ Y. K. Heng,^{1,a} Z. L. Hou,¹ C. Hu,²⁸ H. M. Hu,¹ J. F. Hu,^{49a,49c} T. Hu,^{1,a} Y. Hu,¹ G. M. Huang,⁶ G. S. Huang,^{46,a} J. S. Huang,¹⁵ X. T. Huang,³³ Y. Huang,²⁹ T. Hussain,⁴⁸ Q. Ji,¹ Q. P. Ji,³⁰ X. B. Ji,¹ X. L. Ji,^{1,a} L. W. Jiang,⁵¹ X. S. Jiang,^{1,a} X. Y. Jiang,³⁰ J. B. Jiao,³³ Z. Jiao,¹⁷ D. P. Jin,^{1,a} S. Jin,¹ T. Johansson,⁵⁰ A. Julin,⁴³ N. Kalantar-Nayestanaki,²⁵ X. L. Kang,¹ X. S. Kang,³⁰ M. Kavatsyuk,²⁵ B. C. Ke,⁵ P. Kiese,²² R. Kliemt,¹⁴ B. Kloss,²² O. B. Kolcu,^{40b,i} B. Kopf,⁴ M. Kornicer,⁴² W. Kuehn,²⁴ A. Kupsc,⁵⁰ J. S. Lange,²⁴ M. Lara,¹⁹ P. Larin,¹⁴ C. Leng,^{49c} C. Li,⁵⁰ Cheng Li,^{46,a} D. M. Li,⁵³ F. Li,^{1,a} F. Y. Li,³¹ G. Li,¹ H. B. Li,¹ J. C. Li,¹ Jin Li,³² K. Li,¹³ K. Li,³³ Lei Li,³ P. R. Li,⁴¹ T. Li,³³ W. D. Li,¹ W. G. Li,¹ X. L. Li,³³ X. M. Li,¹² X. N. Li,^{1,a} X. Q. Li,³⁰ Z. B. Li,³⁸ H. Liang,^{46,a} Y. F. Liang,³⁶ Y. T. Liang,²⁴ G. R. Liao,¹¹ D. X. Lin,¹⁴ B. J. Liu,¹ C. X. Liu,¹ D. Liu,^{46,a} F. H. Liu,³⁵ Fang Liu,¹ Feng Liu,⁶ H. B. Liu,¹² H. H. Liu,¹ H. H. Liu,¹⁶ H. M. Liu,¹ J. Liu,¹ J. B. Liu,^{46,a} J. P. Liu,⁵¹ J. Y. Liu,¹ K. Liu,³⁹ K. Y. Liu,²⁷ L. D. Liu,³¹ P. L. Liu,^{1,a} Q. Liu,⁴¹ S. B. Liu,^{46,a} X. Liu,²⁶ Y. B. Liu,³⁰ Z. A. Liu,^{1,a} Zhiqing Liu,²² X. C. Lou,^{1,a,h} H. J. Lu,¹⁷ J. G. Lu,^{1,a} Y. Lu,¹ Y. P. Lu,^{1,a} C. L. Luo,²⁸ M. X. Luo,⁵² T. Luo,⁴² X. L. Luo,^{1,a} X. R. Lyu,⁴¹ F. C. Ma,²⁷ H. L. Ma,¹ L. L. Ma,³³ Q. M. Ma,¹ T. Ma,¹ X. N. Ma,³⁰ X. Y. Ma,^{1,a} F. E. Maas,¹⁴ M. Maggiora,^{49a,49c} Y. J. Mao,³¹ Z. P. Mao,¹ S. Marcello,^{49a,49c} J. G. Messchendorp,²⁵ J. Min,^{1,a} R. E. Mitchell,¹⁹ X. H. Mo,^{1,a} Y. J. Mo,⁶ C. Morales Morales,¹⁴ N. Yu. Muchnoi,^{9,f} H. Muramatsu,⁴³ Y. Nefedov,²³ F. Nerling,¹⁴ I. B. Nikolaev,^{9,f} Z. Ning,^{1,a} S. Nisar,⁸ S. L. Niu,^{1,a} X. Y. Niu,¹ S. L. Olsen,³² Q. Ouyang,^{1,a} S. Pacetti,^{20b} Y. Pan,^{46,a} P. Patteri,^{20a} M. Pelizaeus,⁴ H. P. Peng,^{46,a} K. Peters,¹⁰ J. Pettersson,⁵⁰ J. L. Ping,²⁸ R. G. Ping,¹ R. Poling,⁴³ V. Prasad,¹ H. R. Qi,² M. Qi,²⁹ S. Qian,^{1,a} C. F. Qiao,⁴¹ L. Q. Qin,³³ N. Qin,⁵¹ X. S. Qin,¹ Z. H. Qin,^{1,a} J. F. Qiu,¹ K. H. Rashid,⁴⁸ C. F. Redmer,²² M. Ripka,²² G. Rong,¹ Ch. Rosner,¹⁴ X. D. Ruan,¹² V. Santoro,^{21a} A. Sarantsev,^{23,g} M. Savrié,^{21b} K. Schoenning,⁵⁰ S. Schumann,²² W. Shan,³¹ M. Shao,^{46,a} C. P. Shen,² P. X. Shen,³⁰ X. Y. Shen,¹ H. Y. Sheng,¹ W. M. Song,¹ X. Y. Song,¹ S. Sosio,^{49a,49c} S. Spataro,^{49a,49c} G. X. Sun,¹ J. F. Sun,¹⁵ S. S. Sun,¹ Y. J. Sun,^{46,a} Y. Z. Sun,¹ Z. J. Sun,^{1,a} Z. T. Sun,¹⁹ C. J. Tang,³⁶ X. Tang,¹ I. Tapan,^{40c} E. H. Thorndike,⁴⁴ M. Tiemens,²⁵ M. Ullrich,²⁴ I. Uman,^{40b} G. S. Varner,⁴² B. Wang,³⁰ B. L. Wang,⁴¹ D. Wang,³¹ D. Y. Wang,³¹ K. Wang,^{1,a} L. L. Wang,¹ L. S. Wang,¹ M. Wang,³³ P. Wang,¹ P. L. Wang,¹ S. G. Wang,³¹ W. Wang,^{1,a} W. P. Wang,^{46,a} X. F. Wang,³⁹ Y. D. Wang,¹⁴ Y. F. Wang,^{1,a} Y. Q. Wang,²² Z. Wang,^{1,a} Z. G. Wang,^{1,a} Z. H. Wang,^{46,a} Z. Y. Wang,¹ T. Weber,²² D. H. Wei,¹¹ J. B. Wei,³¹ P. Weidenkaff,²² S. P. Wen,¹ U. Wiedner,⁴ M. Wolke,⁵⁰ L. H. Wu,¹ Z. Wu,^{1,a} L. Xia,^{46,a} L. G. Xia,³⁹ Y. Xia,¹⁸ D. Xiao,¹ H. Xiao,⁴⁷ Z. J. Xiao,²⁸ Y. G. Xie,^{1,a} Q. L. Xiu,^{1,a} G. F. Xu,¹ L. Xu,¹ Q. J. Xu,¹³ Q. N. Xu,⁴¹ X. P. Xu,³⁷ L. Yan,^{49a,49c} W. B. Yan,^{46,a} W. C. Yan,^{46,a} Y. H. Yan,¹⁸ H. J. Yang,³⁴ H. X. Yang,¹ L. Yang,⁵¹ Y. Yang,⁶ Y. X. Yang,¹¹ M. Ye,^{1,a} M. H. Ye,⁷ J. H. Yin,¹ B. X. Yu,^{1,a} C. X. Yu,³⁰ J. S. Yu,²⁶ C. Z. Yuan,¹ W. L. Yuan,²⁹ Y. Yuan,¹ A. Yuncu,^{40b,c} A. A. Zafar,⁴⁸ A. Zallo,^{20a} Y. Zeng,¹⁸ Z. Zeng,^{46,a} B. X. Zhang,¹ B. Y. Zhang,^{1,a} C. Zhang,²⁹ C. C. Zhang,¹ D. H. Zhang,¹ H. H. Zhang,³⁸ H. Y. Zhang,^{1,a} J. J. Zhang,¹ J. L. Zhang,¹ J. Q. Zhang,¹ J. W. Zhang,^{1,a} J. Y. Zhang,¹ J. Z. Zhang,¹ K. Zhang,¹ L. Zhang,¹ X. Y. Zhang,³³ Y. Zhang,¹ Y. H. Zhang,^{1,a} Y. N. Zhang,⁴¹ Y. T. Zhang,^{46,a} Yu Zhang,⁴¹ Z. H. Zhang,⁶ Z. P. Zhang,⁴⁶ Z. Y. Zhang,⁵¹ G. Zhao,¹ J. W. Zhao,^{1,a} J. Y. Zhao,¹ J. Z. Zhao,^{1,a} Lei Zhao,^{46,a} Ling Zhao,¹ M. G. Zhao,³⁰ Q. Zhao,¹ Q. W. Zhao,¹ S. J. Zhao,⁵³ T. C. Zhao,¹ Y. B. Zhao,^{1,a} Z. G. Zhao,^{46,a} A. Zhemchugov,^{23,d} B. Zheng,⁴⁷ J. P. Zheng,^{1,a} W. J. Zheng,³³ Y. H. Zheng,⁴¹ B. Zhong,²⁸ L. Zhou,^{1,a} X. Zhou,⁵¹ X. K. Zhou,^{46,a} X. R. Zhou,^{46,a} X. Y. Zhou,¹ K. Zhu,¹ K. J. Zhu,^{1,a} S. Zhu,¹ S. H. Zhu,⁴⁵ X. L. Zhu,³⁹ Y. C. Zhu,^{46,a} Y. S. Zhu,¹ Z. A. Zhu,¹ J. Zhuang,^{1,a} L. Zotti,^{49a,49c} B. S. Zou,¹ and J. H. Zou¹

(BESIII Collaboration)

- ¹*Institute of High Energy Physics, Beijing 100049, People's Republic of China*
²*Beihang University, Beijing 100191, People's Republic of China*
³*Beijing Institute of Petrochemical Technology, Beijing 102617, People's Republic of China*
⁴*Bochum Ruhr-University, D-44780 Bochum, Germany*
⁵*Carnegie Mellon University, Pittsburgh, Pennsylvania 15213, USA*
⁶*Central China Normal University, Wuhan 430079, People's Republic of China*
⁷*China Center of Advanced Science and Technology, Beijing 100190, People's Republic of China*
⁸*COMSATS Institute of Information Technology, Lahore, Defence Road, Off Raiwind Road, 54000 Lahore, Pakistan*
⁹*G.I. Budker Institute of Nuclear Physics SB RAS (BINP), Novosibirsk 630090, Russia*
¹⁰*GSI Helmholtzcentre for Heavy Ion Research GmbH, D-64291 Darmstadt, Germany*
¹¹*Guangxi Normal University, Guilin 541004, People's Republic of China*
¹²*GuangXi University, Nanning 530004, People's Republic of China*
¹³*Hangzhou Normal University, Hangzhou 310036, People's Republic of China*
¹⁴*Helmholtz Institute Mainz, Johann-Joachim-Becher-Weg 45, D-55099 Mainz, Germany*
¹⁵*Henan Normal University, Xinxiang 453007, People's Republic of China*
¹⁶*Henan University of Science and Technology, Luoyang 471003, People's Republic of China*
¹⁷*Huangshan College, Huangshan 245000, People's Republic of China*
¹⁸*Hunan University, Changsha 410082, People's Republic of China*
¹⁹*Indiana University, Bloomington, Indiana 47405, USA*
^{20a}*INFN Laboratori Nazionali di Frascati, I-00044 Frascati, Italy*
^{20b}*INFN and University of Perugia, I-06100 Perugia, Italy*
^{21a}*INFN Sezione di Ferrara, I-44122 Ferrara, Italy*
^{21b}*University of Ferrara, I-44122 Ferrara, Italy*
²²*Johannes Gutenberg University of Mainz, Johann-Joachim-Becher-Weg 45, D-55099 Mainz, Germany*
²³*Joint Institute for Nuclear Research, 141980 Dubna, Moscow region, Russia*
²⁴*Justus Liebig University Giessen, II. Physikalisches Institut, Heinrich-Buff-Ring 16, D-35392 Giessen, Germany*
²⁵*KVI-CART, University of Groningen, NL-9747 AA Groningen, The Netherlands*
²⁶*Lanzhou University, Lanzhou 730000, People's Republic of China*
²⁷*Liaoning University, Shenyang 110036, People's Republic of China*
²⁸*Nanjing Normal University, Nanjing 210023, People's Republic of China*
²⁹*Nanjing University, Nanjing 210093, People's Republic of China*
³⁰*Nankai University, Tianjin 300071, People's Republic of China*
³¹*Peking University, Beijing 100871, People's Republic of China*
³²*Seoul National University, Seoul 151-747 Korea*
³³*Shandong University, Jinan 250100, People's Republic of China*
³⁴*Shanghai Jiao Tong University, Shanghai 200240, People's Republic of China*
³⁵*Shanxi University, Taiyuan 030006, People's Republic of China*
³⁶*Sichuan University, Chengdu 610064, People's Republic of China*
³⁷*Soochow University, Suzhou 215006, People's Republic of China*
³⁸*Sun Yat-Sen University, Guangzhou 510275, People's Republic of China*
³⁹*Tsinghua University, Beijing 100084, People's Republic of China*
^{40a}*Istanbul Aydin University, 34295 Sefakoy, Istanbul, Turkey*
^{40b}*Istanbul Bilgi University, 34060 Eyup, Istanbul, Turkey*
^{40c}*Uludag University, 16059 Bursa, Turkey*
⁴¹*University of Chinese Academy of Sciences, Beijing 100049, People's Republic of China*
⁴²*University of Hawaii, Honolulu, Hawaii 96822, USA*
⁴³*University of Minnesota, Minneapolis, Minnesota 55455, USA*
⁴⁴*University of Rochester, Rochester, New York 14627, USA*
⁴⁵*University of Science and Technology Liaoning, Anshan 114051, People's Republic of China*
⁴⁶*University of Science and Technology of China, Hefei 230026, People's Republic of China*
⁴⁷*University of South China, Hengyang 421001, People's Republic of China*
⁴⁸*University of the Punjab, Lahore-54590, Pakistan*
^{49a}*University of Turin, I-10125 Turin, Italy*
^{49b}*University of Eastern Piedmont, I-15121 Alessandria, Italy*
^{49c}*INFN, I-10125 Turin, Italy*
⁵⁰*Uppsala University, Box 516, SE-75120 Uppsala, Sweden*
⁵¹*Wuhan University, Wuhan 430072, People's Republic of China*
⁵²*Zhejiang University, Hangzhou 310027, People's Republic of China*
⁵³*Zhengzhou University, Zhengzhou 450001, People's Republic of China*

(Received 9 October 2015; published 25 November 2015)

We report the first measurement of the absolute branching fraction for $\Lambda_c^+ \rightarrow \Lambda e^+ \nu_e$. This measurement is based on 567 pb^{-1} of e^+e^- annihilation data produced at $\sqrt{s} = 4.599 \text{ GeV}$, which is just above the $\Lambda_c^+ \bar{\Lambda}_c^-$ threshold. The data were collected with the BESIII detector at the BEPCII storage rings. The branching fraction is determined to be $\mathcal{B}(\Lambda_c^+ \rightarrow \Lambda e^+ \nu_e) = [3.63 \pm 0.38(\text{stat}) \pm 0.20(\text{syst})]\%$, representing a significant improvement in precision over the current indirect determination. As the branching fraction for $\Lambda_c^+ \rightarrow \Lambda e^+ \nu_e$ is the benchmark for those of other Λ_c^+ semileptonic channels, our result provides a unique test of different theoretical models, which is the most stringent to date.

DOI: 10.1103/PhysRevLett.115.221805

PACS numbers: 13.30.Ce, 14.20.Lq, 14.65.Dw

Semileptonic (SL) decays of the lightest charmed baryon, Λ_c^+ , provide a stringent test for nonperturbative aspects of the theory of strong interaction. In particular, the decay rate of the most copious SL decay mode, $\Lambda_c^+ \rightarrow \Lambda e^+ \nu_e$, serves as a normalization mode for all other Λ_c^+ SL decay rates. The $\Lambda_c^+ \rightarrow \Lambda e^+ \nu_e$ decay is dominated by the Cabibbo-favored transition $c \rightarrow s l^+ \nu_l$, which occurs, to a good approximation, independently of the spin-zero spectator ud diquark. This leads to a simpler theoretical description and greater predictive power in modeling the SL decays of the charmed baryons than the case for mesons [1]. However, model development for semileptonic decays of charmed mesons is much more advanced because of the availability of experimental data with precision better than 5% [2]. An experimental study of $\Lambda_c^+ \rightarrow \Lambda e^+ \nu_e$ is therefore desirable in order to test different models in the charm baryon sector [3].

Since the first observation of the Λ_c^+ baryon in e^+e^- annihilations at the Mark II experiment [4] in 1979, much theoretical effort has been applied towards the study of its SL decay properties. However, predictions of the branching fraction (BF) $\mathcal{B}(\Lambda_c^+ \rightarrow \Lambda e^+ \nu_e)$ in different theoretical models vary in a wide range from 1.4% to 9.2% [5–15], depending on the choice of various Λ_c^+ wave function models and the nature of decay dynamics. In addition, theoretical calculations prove to be quite challenging for lattice quantum chromodynamics (LQCD) due to the complexity of form factors, which describes the hadronic part of the decay dynamics in $\Lambda_c^+ \rightarrow \Lambda e^+ \nu_e$ [16]. Thus, an accurate measurement of $\mathcal{B}(\Lambda_c^+ \rightarrow \Lambda e^+ \nu_e)$ is a key ingredient in calibrating LQCD calculations, which, in turn, will play an important role in understanding different Λ_c^+ SL decays.

So far, experimental information for $\mathcal{B}(\Lambda_c^+ \rightarrow \Lambda e^+ \nu_e)$ has come only from the ARGUS [17] and CLEO [18] experiments in the 1990s. They measured the product cross section $\sigma(e^+e^- \rightarrow \Lambda_c^+ X) \mathcal{B}(\Lambda_c^+ \rightarrow \Lambda e^+ \nu_e)$ at $B\bar{B}$ threshold energies. Combined with the measured $\mathcal{B}(\Lambda_c^+ \rightarrow p K^- \pi^+) = (6.84 \pm 0.24_{-0.27}^{+0.21})\%$ [19] and the Λ_c^+ lifetime, they evaluated $\mathcal{B}(\Lambda_c^+ \rightarrow \Lambda e^+ \nu_e) = (2.9 \pm 0.5)\%$ [2]. Therefore, this is not a direct determination of $\mathcal{B}(\Lambda_c^+ \rightarrow \Lambda e^+ \nu_e)$. In this Letter, we report the first measurement of the absolute branching fraction for $\Lambda_c^+ \rightarrow \Lambda e^+ \nu_e$, $\mathcal{B}(\Lambda_c^+ \rightarrow \Lambda e^+ \nu_e)$, by analyzing 567 pb^{-1} [20] of data collected at

$\sqrt{s} = 4.599 \text{ GeV}$ by the BESIII detector at the BEPCII collider. This is the largest Λ_c^+ data sample near the $\Lambda_c^+ \bar{\Lambda}_c^-$ threshold, where the Λ_c^+ is always produced in association with a $\bar{\Lambda}_c^-$ baryon. Hence, $\mathcal{B}(\Lambda_c^+ \rightarrow \Lambda e^+ \nu_e)$ can be accessed by measuring the relative probability of finding the SL decay when the $\bar{\Lambda}_c^-$ is reconstructed in a number of prolific decay channels. This will provide a clean and straightforward BF measurement without requiring knowledge of the total number of $\Lambda_c^+ \bar{\Lambda}_c^-$ events produced.

BESIII [21] is a cylindrical spectrometer, which is composed of a helium-gas-based main drift chamber (MDC), a plastic scintillator time-of-flight (TOF) system, a CsI (TI) electromagnetic calorimeter (EMC), a superconducting solenoid providing a 1.0 T magnetic field, and a muon counter. The charged particle momentum resolution is 0.5% at a transverse momentum of 1 GeV/c and the photon energy resolution is 2.5% at 1 GeV. The particle identification (PID) system combines the ionization energy loss (dE/dx) in the MDC, the TOF and EMC information to identify particle types. More details about the design and performance of the detector are given in Ref. [21].

A GEANT4-based [22] Monte Carlo (MC) simulation package, which includes the geometric description of the detector and the detector response, is used to determine the detection efficiency and to estimate the potential backgrounds. Signal MC samples of a Λ_c baryon decaying only to $\Lambda e \nu_e$ together with a $\bar{\Lambda}_c$ decaying only to the studied tag modes are generated by the MC event generator KKMC [23] using EVTGEN [24], with initial-state radiation (ISR) effects [25] and final-state radiation effects [26] included. For the simulation of the decay $\Lambda_c^+ \rightarrow \Lambda e^+ \nu_e$, we use the form factor predictions obtained using heavy quark effective theory and QCD sum rules of Ref. [13]. To study backgrounds, inclusive MC samples consisting of $\Lambda_c^+ \bar{\Lambda}_c^-$ events, $D_{(s)}$ production, ISR return to the charmonium(like) ψ states at lower masses and continuum processes are generated. All decay modes of the Λ_c , ψ , and $D_{(s)}$ as specified in the Particle Data Group (PDG) [2] are simulated by the MC generator. The unknown decays of the ψ states are generated with LUNDCHARM [27].

The technique for this analysis, which was first applied by the Mark III Collaboration [28] at SPEAR, relies on the purity and kinematics of the $\Lambda_c^+ \bar{\Lambda}_c^-$ baryon pairs produced at $\sqrt{s} = 4.599 \text{ GeV}$. First, we select a data sample of $\bar{\Lambda}_c^-$

baryons by reconstructing exclusive hadronic decays; we call this the single tag (ST) sample. Then, we search for $\Lambda_c^+ \rightarrow \Lambda e^+ \nu_e$ in the system recoiling against the ST $\bar{\Lambda}_c^-$ baryons. The ST $\bar{\Lambda}_c^-$ baryons are reconstructed using eleven hadronic decay modes: $\bar{\Lambda}_c^- \rightarrow \bar{p}K_S^0$, $\bar{p}K^+\pi^-$, $\bar{p}K_S^0\pi^0$, $\bar{p}K^+\pi^-\pi^0$, $\bar{p}K_S^0\pi^+\pi^-$, $\bar{\Lambda}\pi^-$, $\bar{\Lambda}\pi^-\pi^0$, $\bar{\Lambda}\pi^-\pi^+\pi^-$, $\bar{\Sigma}^0\pi^-$, $\bar{\Sigma}^-\pi^0$, and $\bar{\Sigma}^-\pi^+\pi^-$, where the intermediate particles K_S^0 , $\bar{\Lambda}$, $\bar{\Sigma}^0$, $\bar{\Sigma}^-$ and π^0 are reconstructed by their decays into $K_S^0 \rightarrow \pi^+\pi^-$, $\bar{\Lambda} \rightarrow \bar{p}\pi^+$, $\bar{\Sigma}^0 \rightarrow \gamma\bar{\Lambda}$ with $\bar{\Lambda} \rightarrow \bar{p}\pi^+$, $\bar{\Sigma}^- \rightarrow \bar{p}\pi^0$, and $\pi^0 \rightarrow \gamma\gamma$, respectively.

Charged tracks are required to have polar angles within $|\cos\theta| < 0.93$, where θ is the polar angle of the charged track with respect to the beam direction. Their distances of closest approach to the interaction point (IP) are required to be less than 10 cm along the beam direction and less than 1 cm in the perpendicular plane. Tracks originating from K_S^0 and Λ decays are not subjected to these distance requirements. To discriminate pions from kaons, the dE/dx and TOF information are used to obtain probabilities for the pion (\mathcal{L}_π) and kaon (\mathcal{L}_K) hypotheses. Pion and kaon candidates are selected using $\mathcal{L}_\pi > \mathcal{L}_K$ and $\mathcal{L}_K > \mathcal{L}_\pi$, respectively. For proton identification, information from dE/dx , TOF, and EMC are combined to calculate the PID probability \mathcal{L}' , and a charged track satisfying $\mathcal{L}'_p > \mathcal{L}'_\pi$ and $\mathcal{L}'_p > \mathcal{L}'_K$ is identified as a proton candidate.

Photon candidates are reconstructed from isolated clusters in the EMC in the regions $|\cos\theta| \leq 0.80$ (barrel) and $0.86 \leq |\cos\theta| \leq 0.92$ (end cap). The deposited energy of a neutral cluster is required to be larger than 25 (50) MeV in barrel (end cap) region, and the angle between the photon candidate and the nearest charged track must be larger than 10° . To suppress electronic noise and energy deposits unrelated to the events, the difference between the EMC time and the event start time is required to be within (0, 700) ns. To reconstruct π^0 candidates, the invariant mass of the accepted photon pairs is required to be within (0.110, 0.155) GeV/ c^2 . A kinematic fit is implemented to constrain the $\gamma\gamma$ invariant mass to the π^0 nominal mass [2], and the χ^2 of the kinematic fit is required to be less than 20. The fitted momenta of the π^0 are used further in the analysis.

To reconstruct K_S^0 and $\bar{\Lambda}$, a secondary vertex fit is applied, and the decay length is required to be larger than zero. The invariant masses $M(\pi^+\pi^-)$, $M(\bar{p}\pi^+)$, $M(\gamma\bar{\Lambda})$, and $M(\bar{p}\pi^0)$ are required to be within (0.485, 0.510) GeV/ c^2 , (1.110, 1.121) GeV/ c^2 , (1.179, 1.205) GeV/ c^2 , and (1.173, 1.200) GeV/ c^2 to select candidates for K_S^0 , $\bar{\Lambda}$, $\bar{\Sigma}^0$, and $\bar{\Sigma}^-$, respectively.

For the ST mode of $\bar{p}K_S^0\pi^0$, $\bar{\Lambda}$, and $\bar{\Sigma}^-$ backgrounds are rejected by vetoing any events with $M(\bar{p}\pi^+)$ and $M(\bar{p}\pi^0)$ inside the regions (1.105, 1.125) GeV/ c^2 and (1.173, 1.200) GeV/ c^2 , respectively. For the ST modes of $\bar{\Lambda}\pi^+\pi^-\pi^-$ and $\bar{\Sigma}^-\pi^+\pi^-$, K_S^0 backgrounds are suppressed

by requiring $M(\pi^+\pi^-)$ outside of (0.480, 0.520) GeV/ c^2 , while Λ backgrounds are removed from decays to $\bar{p}K_S^0\pi^+\pi^-$ and $\bar{\Sigma}^-\pi^+\pi^-$ by requiring $M(\bar{p}\pi^+)$ to be outside of (1.105, 1.125) GeV/ c^2 .

The ST $\bar{\Lambda}_c^-$ signals are identified using the beam constrained mass, $M_{BC} = \sqrt{E_{\text{beam}}^2 - |\vec{p}_{\bar{\Lambda}_c^-}|^2}$, where E_{beam} is the beam energy and $\vec{p}_{\bar{\Lambda}_c^-}$ is the momentum of the $\bar{\Lambda}_c^-$ candidate. To improve the signal purity, the energy difference $\Delta E = E_{\text{beam}} - E_{\bar{\Lambda}_c^-}$ for each candidate is required to be within approximately $\pm 3\sigma_{\Delta E}$ around the ΔE peak, where $\sigma_{\Delta E}$ is the ΔE resolution and $E_{\bar{\Lambda}_c^-}$ is the reconstructed $\bar{\Lambda}_c^-$ energy. The explicit ΔE requirements for different modes are listed in Table I.

The M_{BC} distributions for the eleven $\bar{\Lambda}_c^-$ ST modes are shown in Fig. 1. The ST candidates are selected by further requiring their mass to be within (2.280, 2.296) GeV/ c^2 . To obtain the ST yields, we perform unbinned maximum likelihood fits to the whole mass spectra in Fig. 1, where we use the MC simulated signal shape convoluted with a double-Gaussian resolution function to represent the signal shape and an ARGUS function [29] to describe the background shape. The signal yield is estimated by integrating the fitted signal shape in the mass region (2.280, 2.296) GeV/ c^2 . Peaking backgrounds are evaluated to be $(0.25 \pm 0.04)\%$, according to MC simulations. These backgrounds are subtracted from the fitted number of the singly tagged $\bar{\Lambda}_c^-$ events. The numbers of background-subtracted signal events are used as the ST yields, as listed in Table I. Finally, we obtain the total ST yield summed over all 11 modes to be $N_{\bar{\Lambda}_c^-}^{\text{tot}} = 14415 \pm 159$.

Candidate events for $\Lambda_c^+ \rightarrow \Lambda e^+ \nu_e$ are selected from the remaining tracks recoiling against the ST $\bar{\Lambda}_c^-$ candidates. To select the Λ , the same criteria as those used in the ST

TABLE I. ΔE requirements and ST yields $N_{\bar{\Lambda}_c^-}$ in data.

Mode	ΔE (GeV)	$N_{\bar{\Lambda}_c^-}$
$\bar{p}K_S^0$	[-0.025, 0.028]	1066 ± 33
$\bar{p}K^+\pi^-$	[-0.019, 0.023]	5692 ± 88
$\bar{p}K_S^0\pi^0$	[-0.035, 0.049]	593 ± 41
$\bar{p}K^+\pi^-\pi^0$	[-0.044, 0.052]	1547 ± 61
$\bar{p}K_S^0\pi^+\pi^-$	[-0.029, 0.032]	516 ± 34
$\bar{\Lambda}\pi^-$	[-0.033, 0.035]	593 ± 25
$\bar{\Lambda}\pi^-\pi^0$	[-0.037, 0.052]	1864 ± 56
$\bar{\Lambda}\pi^-\pi^+\pi^-$	[-0.028, 0.030]	674 ± 36
$\bar{\Sigma}^0\pi^-$	[-0.029, 0.032]	532 ± 30
$\bar{\Sigma}^-\pi^0$	[-0.038, 0.062]	329 ± 28
$\bar{\Sigma}^-\pi^+\pi^-$	[-0.049, 0.054]	1009 ± 57

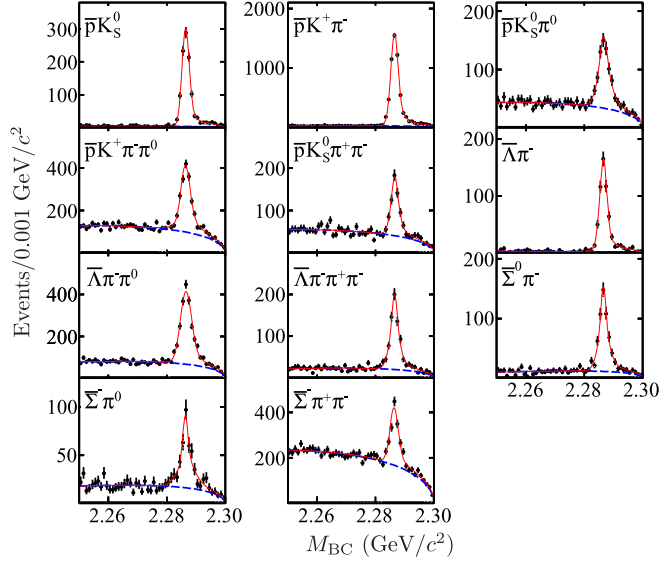


FIG. 1 (color online). Fits to the M_{BC} distributions for different ST modes. The points with error bars are data, the (red) solid curves show the total fits, and the (blue) dashed curves are the background shapes.

selection are applied. We further identify a charged track as an e^+ by requiring the probabilities calculated with the dE/dx , TOF, and EMC satisfying the criteria $\mathcal{L}'_e > 0.001$ and $\mathcal{L}'_e/(\mathcal{L}'_e + \mathcal{L}'_\pi + \mathcal{L}'_K) > 0.8$. Its energy loss due to bremsstrahlung photon(s) is partially recovered by adding the showers that are within a 5° cone about the positron momentum. As the neutrino is not detected, we employ the kinematic variable

$$U_{\text{miss}} = E_{\text{miss}} - c|\vec{p}_{\text{miss}}|$$

to obtain information on the neutrino, where E_{miss} and \vec{p}_{miss} are the missing energy and momentum carried by the neutrino, respectively. They are calculated by $E_{\text{miss}} = E_{\text{beam}} - E_\Lambda - E_{e^+}$ and $\vec{p}_{\text{miss}} = \vec{p}_{\Lambda_c^+} - \vec{p}_\Lambda - \vec{p}_{e^+}$, where $\vec{p}_{\Lambda_c^+}$ is the momentum of Λ_c^+ baryon, and $E_\Lambda(\vec{p}_\Lambda)$ and $E_{e^+}(\vec{p}_{e^+})$ are the energies (momenta) of the Λ and the positron, respectively. Here, the momentum $\vec{p}_{\Lambda_c^+}$ is given by $\vec{p}_{\Lambda_c^+} = -\hat{p}_{\text{tag}} \sqrt{E_{\text{beam}}^2 - m_{\bar{\Lambda}_c^-}^2}$, where \hat{p}_{tag} is the direction of the momentum of the ST $\bar{\Lambda}_c^-$ and $m_{\bar{\Lambda}_c^-}$ is the nominal $\bar{\Lambda}_c^-$ mass [2]. For signal events, U_{miss} is expected to peak around zero.

Figure 2(a) shows a scatter plot of $M_{p\pi^-}$ versus U_{miss} for the $\Lambda_c^+ \rightarrow \Lambda e^+ \nu_e$ candidates in data. Most of the events are located around the intersection of the Λ and $\Lambda e^+ \nu_e$ signal regions. Requiring $M_{p\pi^-}$ to be within the Λ signal region, we project the scatter plot onto the U_{miss} axis, as shown in Fig. 2(b). The U_{miss} distribution is fitted with a signal function f plus a flat function to describe the background. The signal function f [30] consists of a Gaussian function to model the

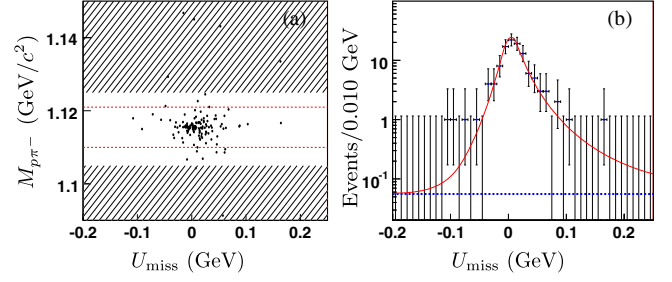


FIG. 2 (color online). (a) Scatter plot of $M_{p\pi^-}$ versus U_{miss} for the $\Lambda_c^+ \rightarrow \Lambda e^+ \nu_e$ candidates. The area between the dashed lines denotes the Λ signal region and the hatched areas indicate the Λ sideband regions. (b) Fit to the U_{miss} distribution within the Λ signal region. The points with error bars are data, the (red) solid curve shows the total fit, and the (blue) dashed curve is the background shape.

core of the U_{miss} distribution and two power law tails to account for the effects of initial- and final-state radiation:

$$f(U_{\text{miss}}) = \begin{cases} p_1 \left(\frac{n_1}{\alpha_1} - \alpha_1 + t \right)^{-n_1}, & t > \alpha_1 \\ e^{-t^2/2}, & -\alpha_2 < t < \alpha_1 \\ p_2 \left(\frac{n_2}{\alpha_2} - \alpha_2 - t \right)^{-n_2}, & t < -\alpha_2 \end{cases} \quad (1)$$

where $t = (U_{\text{miss}} - U_{\text{mean}})/\sigma_{U_{\text{miss}}}$, U_{mean} , and $\sigma_{U_{\text{miss}}}$ are the mean value and resolution of the Gaussian function, respectively, $p_1 \equiv (n_1/\alpha_1)^{n_1} e^{-\alpha_1^2/2}$ and $p_2 \equiv (n_2/\alpha_2)^{n_2} e^{-\alpha_2^2/2}$. The parameters α_1 , α_2 , n_1 , and n_2 are fixed to the values obtained in the signal MC simulations. From the fit, we obtain the number of SL signals to be 109.4 ± 10.9 .

The backgrounds in $\Lambda_c^+ \rightarrow \Lambda e^+ \nu_e$ arise mostly from misreconstructed SL decays with correctly reconstructed tags. There are two types of peaking backgrounds. The first comes from non- Λ SL decays, which are studied using data in the Λ sideband in Fig. 2. We obtain the number of events of the first type of backgrounds to be 1.4 ± 0.8 , after scaling to the Λ signal region. The second peaking background arises from $\Lambda_c^+ \rightarrow \Lambda \mu^+ \nu_\mu$ and some hadronic decays, such as $\Lambda_c^+ \rightarrow \Lambda \pi^+ \pi^0$, $\Lambda \pi^+$, and $\Sigma^0 \pi^+$. Based on MC simulations, we determine the number of background events of the second type to be 4.5 ± 0.5 . After subtracting these background events, we determine the net number of $\Lambda_c^+ \rightarrow \Lambda e^+ \nu_e$ to be $N_{\text{semi}} = 103.5 \pm 10.9$, where the uncertainty is statistical.

The absolute BF for $\Lambda_c^+ \rightarrow \Lambda e^+ \nu_e$ is determined by

$$\mathcal{B}(\Lambda_c^+ \rightarrow \Lambda e^+ \nu_e) = \frac{N_{\text{semi}}}{N_{\Lambda_c^+}^{\text{tot}} \times \varepsilon_{\text{semi}} \times \mathcal{B}(\Lambda \rightarrow p\pi^-)}, \quad (2)$$

where $\varepsilon_{\text{semi}} = (30.92 \pm 0.26)\%$, which does not include the BF for $\Lambda \rightarrow p\pi^-$, is the overall efficiency for detecting the $\Lambda_c^+ \rightarrow \Lambda e^+ \nu_e$ decay in ST events, weighted by the ST

yields of data for each tag. Inserting the values of N_{semi} , $N_{\Lambda_c^+}^{\text{tot}}$, ϵ_{semi} , and $\mathcal{B}(\Lambda \rightarrow p\pi^-)$ [2] in Eq. (2), we get $\mathcal{B}(\Lambda_c^+ \rightarrow \Lambda e^+\nu_e) = (3.63 \pm 0.38 \pm 0.20)\%$, where the first error is statistical and the second systematic.

The systematic error [31] is mainly due to the uncertainty in the efficiency of Λ reconstruction (2.5%), which is studied with $\chi_{cJ} \rightarrow \Lambda \bar{\Lambda} \pi^+ \pi^-$, and the simulation of the SL signal model (4.5%), estimated by changing the default parametrization of form factor function to other parameters in Refs. [13,32] and by taking into account the q^2 dependence observed in data. Other relevant issues include the following uncertainties: the electron tracking (1.0%) and the electron PID (1.0%) which is studied with $e^+e^- \rightarrow (\gamma)e^+e^-$, the fit to the U_{miss} distribution (0.8%) estimated by using alternative signal shapes, the quoted BF for $\Lambda \rightarrow p\pi^-$ (0.8%), the MC statistics (0.8%), the background subtraction (0.5%), and the $N_{\Lambda_c^-}$ (1.0%) evaluated by using alternative signal shapes in the fits to the M_{BC} spectra. The total systematic error is estimated to be 5.6% by adding all these uncertainties in quadrature.

In summary, we report the first measurement of the absolute BF for $\Lambda_c^+ \rightarrow \Lambda e^+\nu_e$, $\mathcal{B}(\Lambda_c^+ \rightarrow \Lambda e^+\nu_e) = (3.63 \pm 0.38 \pm 0.20)\%$, based on 567 pb^{-1} data taken at $\sqrt{s} = 4.599$ GeV. This work improves the precision of the world average value more than twofold. As the theoretical predictions on this rate vary in a large range of 1.4%–9.2% [5–15], our result thus provide a stringent test on these nonperturbative models. At a confidence level of 95%, this measurement disfavors the predictions in Refs. [5–9].

The BESIII Collaboration thanks the staff of BEPCII and the IHEP computing center for their strong support. This work is supported in part by National Key Basic Research Program of China under Contract No. 2015CB856700; National Natural Science Foundation of China (NSFC) under Contracts No. 11125525, No. 11235011, No. 11275266, No. 11322544, No. 11322544, No. 11335008, No. 11425524, and No. 11505010; the Chinese Academy of Sciences (CAS) Large-Scale Scientific Facility Program; the CAS Center for Excellence in Particle Physics (CCEPP); the Collaborative Innovation Center for Particles and Interactions (CICPI); Joint Large-Scale Scientific Facility Funds of the NSFC and CAS under Contracts No. 11179007, No. U1232201, and No. U1332201; CAS under Contracts No. KJCX2-YW-N29 and No. KJCX2-YW-N45; 100 Talents Program of CAS; National 1000 Talents Program of China; INPAC and Shanghai Key Laboratory for Particle Physics and Cosmology; German Research Foundation DFG under Contract No. Collaborative Research Center CRC-1044; Istituto Nazionale di Fisica Nucleare, Italy; Koninklijke Nederlandse Akademie van Wetenschappen (KNAW) under Contract No. 530-4CDP03; Ministry of Development of Turkey under Contract No. DPT2006K-120470; Russian Foundation for Basic Research under Contract No. 14-07-91152; The Swedish Resarch Council;

U. S. Department of Energy under Contracts No. DE-FG02-04ER41291, No. DE-FG02-05ER41374, No. DE-SC0012069, and No. DESC0010118; U.S. National Science Foundation; University of Groningen (RuG) and the Helmholtzzentrum fuer Schwerionenforschung GmbH (GSI), Darmstadt; and WCU Program of National Research Foundation of Korea under Contract No. R32-2008-000-10155-0.

^aAlso at State Key Laboratory of Particle Detection and Electronics, Beijing 100049, Hefei 230026, People's Republic of China.

^bAlso at Ankara University, 06100 Tandogan, Ankara, Turkey.

^cAlso at Bogazici University, 34342 Istanbul, Turkey.

^dAlso at the Moscow Institute of Physics and Technology, Moscow 141700, Russia.

^eAlso at the Functional Electronics Laboratory, Tomsk State University, Tomsk, 634050, Russia.

^fAlso at the Novosibirsk State University, Novosibirsk, 630090, Russia.

^gAlso at the NRC “Kurchatov Institute”, PNPI, 188300, Gatchina, Russia.

^hAlso at University of Texas at Dallas, Richardson, TX 75083, USA.

ⁱAlso at Istanbul Arel University, 34295 Istanbul, Turkey.

- [1] J. D. Richman and P. R. Burchat, *Rev. Mod. Phys.* **67**, 893 (1995); E. Eichten and B. Hill, *Phys. Lett. B* **234**, 511 (1990); M. Neubert, *Phys. Rep.* **245**, 259 (1994).
- [2] K. A. Olive *et al.* (Particle Data Group), *Chin. Phys. C* **38**, 090001 (2014) and 2015 update.
- [3] Throughout the text, the inclusion of charge conjugated processes is always implied.
- [4] G. S. Abrams *et al.* (Mark II Collaboration), *Phys. Rev. Lett.* **44**, 10 (1980).
- [5] R. Perez-Marcial, R. Huerta, A. Garcia, and M. Avila-Aoki, *Phys. Rev. D* **40**, 2955 (1989).
- [6] M. Avila-Aoki, A. Garcia, R. Huerta, and R. Perez-Marcial, *Phys. Rev. D* **40**, 2944 (1989).
- [7] G. V. Efimov, M. A. Ivanov, and V. E. Lyubovitskij, *Z. Phys. C* **52**, 149 (1991).
- [8] R. Singleton, Jr., *Phys. Rev. D* **43**, 2939 (1991).
- [9] A. Garcia and R. Huerta, *Phys. Rev. D* **45**, 3266 (1992).
- [10] H. Y. Cheng and B. Tseng, *Phys. Rev. D* **53**, 1457 (1996).
- [11] F. Hussain, and J. G. Körner, *Z. Phys. C* **51**, 607 (1991).
- [12] H. G. Dosch, E. Ferreira, M. Nielsen, and R. Rosenfeld, *Phys. Lett. B* **431**, 173 (1998).
- [13] R. S. Marques de Carvalho, F. S. Navarra, M. Nielsen, E. Ferreira, and H. G. Dosch, *Phys. Rev. D* **60**, 034009 (1999).
- [14] M. Pervin, W. Roberts, and S. Capstick, *Phys. Rev. C* **72**, 035201 (2005).
- [15] Y. L. Liu, M. Q. Huang, and D. W. Wang, *Phys. Rev. D* **80**, 074011 (2009).
- [16] J. L. Rosner, *Phys. Rev. D* **86**, 014017 (2012).
- [17] H. Albrecht *et al.* (ARGUS Collaboration), *Phys. Lett. B* **269**, 234 (1991).

- [18] T. Bergfeld *et al.* (CLEO Collaboration), *Phys. Lett. B* **323**, 219 (1994); G. D. Crawford *et al.* (CLEO Collaboration), *Phys. Rev. Lett.* **75**, 624 (1995);
- [19] A. Zupanc *et al.* (Belle Collaboration), *Phys. Rev. Lett.* **113**, 042002 (2014).
- [20] M. Ablikim *et al.* (BESIII Collaboration), *Chin. Phys. C* **39**, 093001 (2015).
- [21] M. Ablikim *et al.* (BESIII Collaboration), *Nucl. Instrum. Methods Phys. Res., Sect. A* **614**, 345 (2010).
- [22] S. Agostinelli *et al.* (GEANT4 Collaboration), *Nucl. Instrum. Methods Phys. Res., Sect. A* **506**, 250 (2003).
- [23] S. Jadach, B. F. L. Ward, and Z. Was, *Comput. Phys. Commun.* **130**, 260 (2000); *Phys. Rev. D* **63**, 113009 (2001).
- [24] D. J. Lange, *Nucl. Instrum. Methods Phys. Res., Sect. A* **462**, 152 (2001); R. G. Ping, *Chin. Phys. C* **32**, 599 (2008).
- [25] E. A. Kuraev and V. S. Fadin, *Sov. J. Nucl. Phys.* **41**, 466 (1985) [*Yad. Fiz.* **41**, 733 (1985)].
- [26] E. Richter-Was, *Phys. Lett. B* **303**, 163 (1993).
- [27] J. C. Chen, G. S. Huang, X. R. Qi, D. H. Zhang, and Y. S. Zhu, *Phys. Rev. D* **62**, 034003 (2000).
- [28] J. Adler *et al.* (Mark III Collaboration), *Phys. Rev. Lett.* **62**, 1821 (1989).
- [29] H. Albrecht *et al.* (ARGUS Collaboration), *Phys. Lett. B* **241**, 278 (1990).
- [30] J. Y. Ge *et al.* (CLEO Collaboration), *Phys. Rev. D* **79**, 052010 (2009).
- [31] The percentages quoted for the systematic uncertainties in this paragraph are relative to the measured BF.
- [32] J. W. Hinson *et al.* (CLEO Collaboration), *Phys. Rev. Lett.* **94**, 191801 (2005).